Applied Catalysis B: Environmental 95 (2010) 93–99

Contents lists available at ScienceDirect

Applied Catalysis B: Environmental

journal homepage: www.elsevier.com/locate/apcatb

Supported cobalt oxide on MgO: Highly efficient catalysts for degradation of organic dyes in dilute solutions

Wei Zhang [a], Hui Lin Tay [a], Sze Sheng Lim [a], Yongsheng Wang [b], Ziyi Zhong [c], Rong Xu [a,*]

[a] School of Chemical & Biomedical Engineering, Nanyang Technological University, 62 Nanyang Drive, Singapore 637459, Singapore
[b] School of Mechanical & Aerospace Engineering, Nanyang Technological University, 50 Nanyang Avenue, Singapore 639798, Singapore
[c] Institute of Chemical & Engineering Sciences, Agency for Science, Technology and Research (A-Star), No. 1, Pesek Road, Jurong Island, Singapore 627833, Singapore

ARTICLE INFO

Article history:
Received 9 October 2009
Received in revised form 5 December 2009
Accepted 16 December 2009
Available online 23 December 2009

Keywords:
Advanced oxidation technologies (AOTs)
Peroxymonosulfate (PMS)
Oxone
Sulfate radicals
Cobalt oxides
Magnesium oxide (MgO)
Support materials
Organic dyes
Methylene blue (MB)
Orange II
Malachite green

ABSTRACT

Cobalt oxide catalysts immobilized on various oxides (MgO, ZnO, Al_2O_3, ZrO_2, P25, SBA-15) were prepared for degradation of organic dyes in dilute solutions via a sulfate radical approach. Their efficiency in activation of peroxymonosulfate (PMS) was investigated for the degradation of methylene blue (MB). Among the catalysts employed, the Co/MgO catalyst was found the most active. The complete degradation of MB occurred in <7 min when the Co/MgO catalyst with an optimum Co_3O_4 loading of 5 wt% was used. The performance of the Co/MgO catalyst is found better than both the homogeneous cobalt ions and heterogeneous Co_3O_4 catalyst. XPS analysis indicates that the surface of the MgO support is extensively covered by the hydroxyl groups. Hence, it is suggested that the alkaline MgO support plays several important roles in (i) dispersing the cobalt oxide nanoparticles well, (ii) minimizing the leaching of cobalt ions into the liquid phase, and (iii) facilitating the formation of surface Co–OH complex which is a critical step for PMS activation. Besides MB, other organic dyes such as orange II and malachite green, can also be degraded within a few minutes using the Co/MgO catalyst. It is believed that the highly efficient and environmentally benign Co/MgO catalyst developed in this work can be widely applied in advanced oxidation technologies towards degradation of organic pollutants.

© 2009 Elsevier B.V. All rights reserved.

1. Introduction

Due to more stringent statutory regulations and increasing public concerns on harmful organic substances, there is an imperative need to develop efficient technologies for the complete removal of organic pollutants from wastewater effluents. Over the past years, sulfate radicals based-advanced oxidation technologies (SRs-AOTs) have emerged as a promising way leading to the total mineralization of most organic pollutants [1–3]. Oxone (peroxymonosulfate, PMS, as the active component) has been widely used in oxidation of organic pollutants due to its stability and ease of handling compared to H_2O_2 [2,4–12]. This highly active oxidant has also been used in biochemistry [13] and polymer [14] industry to provide reaction initialization radicals. It has been reported that the coupling of transition metal ions like Fe^{2+}, Cu^{2+}, Mn^{2+} and Co^{2+}, to PMS leads to the accelerated generation of SRs and hence higher oxidation efficiencies [3,7,15]. The various combinations between the dissolved transition metal ions and oxidants have been systematically evaluated for the generation of active radicals by Anipsitakis and co-workers. It was found that PMS coupled with Co^{2+} ions is the best combination for the generation of SRs for degrading 2,4-dichlorophenol (2,4-DCP) [3]. However, the potential health hazards caused by the dissolved Co^{2+} ions in water render such a homogeneous Co^{2+}/PMS system with limited use. Therefore, the activation of PMS by heterogeneous cobalt sources has been given great attention recently. Dionysiou and co-workers studied both the unsupported Co_3O_4 and supported Co_3O_4 on several common supports (Al_2O_3, SiO_2, TiO_2) as the heterogeneous activators for PMS to degrade 2,4-DCP [10,11,16]. Kiwi and co-workers used polytetrafluoroethylene flexible film as the support for Co_3O_4 nanoparticles to decompose organic dyes under light irradiation [9]. Chen et al. evaluated the performance of unsupported Co_3O_4 nanoparticles [12].

Besides playing important roles in dispersing the Co_3O_4 nanoparticles and minimizing the leaching of cobalt ions into the liquid phase, support materials also facilitate the formation of surface Co–OH complex which is the critical step for heterogeneous activation of PMS [11,12,16]. In particular, it has been reported that TiO_2 plays a significant role in promoting this step [11]. As the surface properties vary extensively among different

* Corresponding author.
E-mail address: rxu@ntu.edu.sg (R. Xu).

0926-3373/$ – see front matter © 2009 Elsevier B.V. All rights reserved.
doi:10.1016/j.apcatb.2009.12.014

support materials, it is worthwhile to further study the effects of different supports for the development of efficient oxidation catalysts. To meet the ever rising environmental challenges, the desirable heterogeneous cobalt catalysts should offer higher activation efficiencies than the homogeneous Co^{2+} ions, as well as good operational stability.

MgO is frequently employed as an alkaline catalyst for some reactions of commercial importance [17–19]. The abundant surface basic sites on MgO are expected to generate the surface functional Co–OH complex. Herein, we report cobalt oxide supported on MgO (Co/MgO) as an efficient heterogeneous catalyst for activation of PMS. A series of other commonly available support materials including Al_2O_3, P25–TiO_2, SBA-15 (mesoporous SiO_2), ZnO and ZrO_2 were used for comparison. Their activities were measured and compared in the degradation of methylene blue (MB), which is a cationic, non-biodegradable and toxic dye used extensively in dying industry [20–23]. It has been found that the Co/MgO catalyst is able to completely degrade MB and other organic dyes in dilute solutions within a very short duration of a few minutes without light irradiation. The current catalyst system is therefore expected to be highly desirable for competing with the conventional nondestructive treatment processes.

2. Experimental

2.1. Preparation of catalysts

The support materials ZnO (Kanto Chemical, 99%) and P25 titania (Degussa, >99.5%) were obtained from commercial suppliers and used without further purification. MgO and Al_2O_3 were obtained after calcination of commercial $Mg(OH)_2$ (Fluka, >99%) and $Al(OH)_3$ (Riedei-de Haen, Al content 63–67%), respectively in static air at 400 °C for 3 h. ZrO_2 was obtained by calcination of zirconium oxyhydroxide which was prepared by precipitation of $ZrOCl_2$ (Kanto Chemical, 99%) using ammonia (Kanto Chemical, 28–30% in water) according to the procedures described in a previous report [24] in static air at 400 °C for 3 h. SBA-15 was obtained from Dr. Y.H. Yang Research Lab, which was prepared according to their reported method in the literature [25]. The catalysts of cobalt oxide supported on various metal oxides were prepared by incipient wetness impregnation with an aqueous solution of $Co(NO_3)_2{\cdot}6H_2O$ (cobalt nitrate hexahydrate, Fluka Chemika, >99%), followed by drying at 60 °C overnight and then calcination at 600 °C for 3 h in static air. To study the effect of calcination temperature, MgO supported cobalt catalyst was also calcined at 400 and 800 °C. The unsupported Co_3O_4 catalyst was prepared by calcination of $Co(NO_3)_2{\cdot}6H_2O$ at 600 °C for 3 h in static air.

2.2. Catalyst characterization

The powder X-ray diffraction (XRD) patterns of as-prepared samples were recorded on a Bruker AXS D8 X-ray diffractometer with Cu Kα (λ = 1.5406 Å) radiation at 40 kV and 20 mA. The BET surface areas were measured in Autosorb-6B (Quantachrome Instruments) using the liquid nitrogen adsorption method. The leached Co^{2+} ion concentration was measured by inductively coupled plasma (ICP) optical emission spectroscopy on a Prodigy High Dispersion ICP (Leeman Teledyne). Solutions were taken during the reactions, filtered and mixed with 2% nitric acid aqueous solution before analysis. The morphology and nanocrystal sizes were measured by transmission electron microscope (TEM) in JEOL 2010 with an accelerating voltage of 200 kV. X-ray photoelectron spectroscopy (XPS) analysis was conducted in an Axis Ultra Spectrometer (Kratos Analytical) using a monochromated Al Kα X-ray source (1486.7 eV) operating at 15 kV. The binding energies were calibrated with the position of C 1s peak at 284.6 eV arising from the adventitious hydrocarbon.

2.3. Evaluation of catalytic activity

In a typical reaction of methylene blue (MB, Alfa Aesar, high purity) degradation, 10 mg of catalyst and 0.1 mmol of oxone (0.5 mM, $2KHSO_5{\cdot}KHSO_4{\cdot}K_2SO_4$, Alfa Aesar, 4.7% active oxygen) were added in 200 mL of MB solution. The starting concentration of MB was 40 ppm (~15 mg/L, 1 ppm = 1 μM). The reaction was conducted in a beaker with constant stirring at around 300 rpm. The beaker was covered and wrapped with aluminum foil to block the incidence of indoor light to the reaction mixture. At certain reaction time intervals, liquids of about 1 mL were withdrawn from the suspension and then filtered. The measurement of MB concentration in the filtrate was carried out in a UV–vis spectrophotometer (Shimadzu 2450). The area of the absorption bands integrated in the range of 500–750 nm was used to monitor the reaction progress. The activity of the Co/MgO catalyst was also evaluated for the degradation of orange II and malachite green under the same experimental conditions. For the recycle runs of MB degradation, the used catalyst was collected by centrifugation, washed thoroughly and dried at 60 °C overnight before the next run. Due to the small particle sizes, certain catalyst loss was unavoidable during the washing and drying process. Therefore, several parallel reactions were conducted in the first and second runs to ensure that the recycled catalyst amount was enough for the next run. Catalyst dose and other reaction conditions remained the same for the subsequent runs. Altogether three runs conducted for this type of recycle study. To further evaluate the stability of the catalyst in a greater number of recycle runs, a higher catalyst dose (0.2 g) was used for the reaction while keeping other conditions the same. After the complete decolorization of the MB solution, the catalyst was collected by centrifugation and washed with deionized water three times before the next run. The reactions were repeated for 10 times. The final catalyst was collected by centrifugation, washed thoroughly and dried at 60 °C overnight. Then 10 mg of the dried catalyst was used for the last reaction run under the same conditions.

3. Results and discussion

3.1. Catalyst properties

Fig. 1 displays the XRD patterns of the calcined cobalt catalysts supported on various oxide materials together with the standard line pattern of Co_3O_4 (JCPDS #42-1467). The BET surface areas of these catalysts are summarized in Table 1. The loading of Co_3O_4 on different supports was fixed at 5 wt%. It can be observed that although after being calcined at 600 °C in air for 3 h, the catalysts do not exhibit strong diffraction peaks of Co_3O_4 phase due to a low Co_3O_4 loading percentage. Among the samples, Co/Al_2O_3 (Fig. 1a) and Co/SBA-15 (Fig. 1b) show very weak diffraction of Co_3O_4 phase, and Co/ZnO (Fig. 1f) exhibits slightly stronger diffraction of Co_3O_4. In the rest of the samples, Co_3O_4 phase is either not observable for Co/MgO (Fig. 1e) or extremely weak for Co/P25 (Fig. 1c) and Co/ZrO_2 (Fig. 1d). The specific surface area (S.S.A.) and the surface property are the important factors which determine the dispersion of the active phase of the catalysts. ZnO has the lowest S.S.A. of 18.7 m^2/g, which leads to the relatively poor dispersion of cobalt species and hence larger crystallites upon calcination. It has been widely reported that the acidity of the oxides follows the order of $SiO_2 > \gamma\text{-}Al_2O_3 > TiO_2 > ZrO_2 > ZnO > MgO$ [26,27]. Although the S.S.A. of Al_2O_3 and SBA-15 is among the highest at around 180 and 546 m^2/g, respectively, their acidic surface favors the segregation of cobalt phases since Co^{2+} cations can be considered as a Lewis

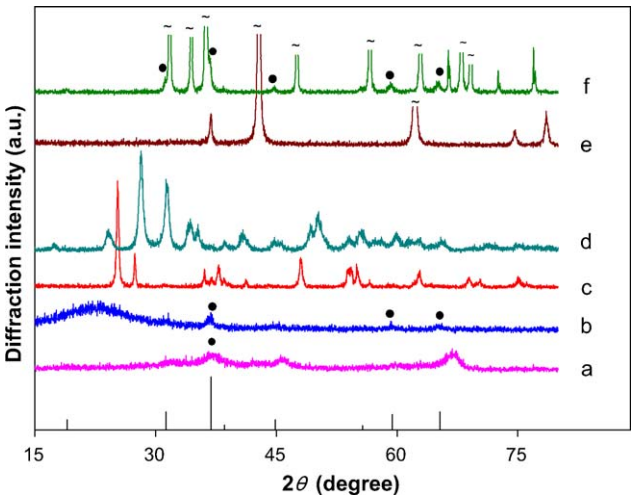

Fig. 1. XRD patterns of (a) Co/Al_2O_3, (b) Co/SBA-15, (c) Co/P25, (d) Co/ZrO_2, (e) Co/MgO, and (f) Co/ZnO. The loading of Co_3O_4 was 5 wt%. The diffraction peaks of Co_3O_4 phase are labeled with •. The line pattern belongs to the standard Co_3O_4 phase (JCPDS #42-1467).

acid [28]. On the other hand, MgO is an alkaline support. The basic sites on the surface of MgO promote the good dispersion of Co^{2+} cations during the impregnation and as a result, no crystalline Co_3O_4 phase can be observed in Co/MgO. The other two supports, P25 and ZrO_2, have a weaker acidic surface compared to Al_2O_3 and SBA-15. Therefore, better dispersion of cobalt species could be resulted and Co_3O_4 phase is almost not observable on these two supports. The rest of the diffraction peaks in Fig. 1 can be readily assigned to the respective phases of the support materials, γ-Al_2O_3, amorphous SiO_2, TiO_2 (anatase and rutile), ZrO_2 (tetragonal and monoclinic), MgO (cubic) and ZnO (hexagonal).

Although not detectable by the XRD technique, the presence of cobalt oxide nanoparticles in Co/MgO can be confirmed based on the TEM and HRTEM images. As observed in Fig. 2a, the sample exhibits irregularly shaped MgO particles of 50–200 nm in size. Some dark spots as pointed out by the arrows should be cobalt oxide nanoparticles based on the *Z*-contrast since cobalt is a heavier element than magnesium. It can be seen that cobalt oxide nanoparticles are well dispersed on the surface of MgO support. The sizes of majority of cobalt oxide nanoparticles fall in a range of 5–10 nm and the remaining small portion has larger particle sizes of around 20 nm. The image taken at a higher magnification (Fig. 2b) indicates that cobalt oxide nanoparticles have an intimate contact with the support MgO particle. The two selected areas inside the boxes in Fig. 2b were further analyzed with HRTEM technique. As shown in Fig. 2c, two types of lattices can be distinguished. The upper part of the image displays a lattice distance of 0.21 nm which can be assigned to the (2 2 0) planes of cubic phased MgO. The lower left portion of the image shows a lattice distance of 0.17 nm which corresponds to the (4 2 2) planes of the cubic spinel Co_3O_4. A similar observation can be made in Fig. 2d with MgO and Co_3O_4 phases identified. Based on the HRTEM images, it is important to note that no distinct boundaries are present between these two phases, indicating that a good interaction exists between the cobalt oxide phase and the MgO support materials.

The XPS spectra of the surface oxygen and metal species in samples MgO, Co/MgO and Co/Al_2O_3 are displayed in Figs. 3 and 4. It can be seen that MgO and Co/MgO give similar spectra for both O 1s and Mg 2p. As shown in Fig. 3a, two O 1s subpeaks can be resolved with their BEs at 531.1 and 529.0 eV, which shall be assigned to oxygen of the hydroxyl and oxide groups, respectively [29]. Based on the peak areas, the ratio of hydroxyl and oxide groups is calculated to be 83:17, indicating that the surface of MgO is dominantly covered by the hydroxyl group. It has been commonly known that upon exposure to moisture, the surface of most oxides is hydroxylated due to dissociative chemisorption of water [30]. The extent of hydroxylation of metal oxide surface depends on the chemistry of the metal ions involved [31]. MgO is considered a strongly basic oxide material with a high isoelectric point of 11.8 [32]. Therefore, it is not surprised to have its surface covered extensively by the hydroxyl groups. On the surface of Co/MgO, the ratio of hydroxyl to oxide group is slightly decreased to 79:21 due to the contribution of oxide from the cobalt oxide species. The spectra of Mg 2p of these two samples consistently show that majority of the Mg^{2+} ions are coordinated with the hydroxyl group (peak at 49.1 eV in Fig. 3d and e) [29]. The peak at higher BEs of 50.4 and 50.3 eV denotes Mg^{2+} in the oxide environment [29]. On the other hand, the O 1s pattern of Co/Al_2O_3 is distinctively different. As shown in Fig. 3c, the main O 1s peak with a BE of 530.5 eV is attributed to oxygen in γ-Al_2O_3 [29,33]. The small peak at 532.1 eV could be due to the oxygen in either α-Al_2O_3 or hydroxyl group [29]. However, the spectrum of Al 2p shown in Fig. 3f indicates the absence of Al^{3+} coordinated to hydroxyl group which should have a lower BE than 73.9 eV. The major peak at this BE can be readily assigned to Al^{3+} in γ-Al_2O_3 oxide and a minor peak at 75.2 to α-Al_2O_3 oxide [34,35]. Therefore, unlike MgO, the Al_2O_3 surface is mainly covered by the oxide. The XPS spectra of Co 2p are shown in Fig. 4. As the BE of cobalt in Co_3O_4 is normally at 779.9 eV [36], the major peak with a higher BE at 780.4 eV (peak 1) for Co $2p_{3/2}$ in sample Co/MgO (Fig. 4a) can be possibly assigned to the cobalt cations coordinated to hydroxyl groups due to the chemical shift [11]. This is in agreement with the presence of the abundant surface hydroxyl groups based on the spectra of O 1s and Mg 2p discussed earlier, which leads to the formation of Co–OH complex. The minor peak at a higher BE of 783.5 eV (peak 2) could be attributed to cobalt cations in association with the residual nitrate anions, as they can be re-adsorbed on the surface of the catalyst during calcination [36]. The two corresponding shake-up satellite peaks are centered at 786.9 eV (peak 1′) and 789.0 eV (peak 2′) respectively [36,37]. On the other hand, the BE of the major peak for Co $2p_{3/2}$ in sample Co/Al_2O_3 is at 780.1 eV which is quite close to that of Co_3O_4 phase (779. 9 eV). This is in agreement with the oxide environment on the surface of the Al_2O_3 support.

Table 1
Supported cobalt oxide catalysts studied in this work and their BET surface areas.

Catalyst	Support preparation method	Calcination conditions	BET S.S.A. (m^2/g)
Co/MgO	Calcination of commercial $Mg(OH)_2$ at 400 °C, 3 h	400 °C, 3 h	75.8
		600 °C, 3 h	74.6
		800 °C, 3 h	41.3
Co/Al_2O_3	Calcination of commercial $Al(OH)_3$ at 400 °C, 3 h	600 °C, 3 h	180.2
Co/ZrO_2	Precipitation of $ZrOCl_2$ by ammonia, followed by calcination at 400 °C, 3 h [24]	600 °C, 3 h	38.3
Co/ZnO	Commercial	600 °C, 3 h	18.7
Co/P25	Commercial	600 °C, 3 h	37.0
Co/SBA-15	Template-assisted synthesis [25]	600 °C, 3 h	546.3

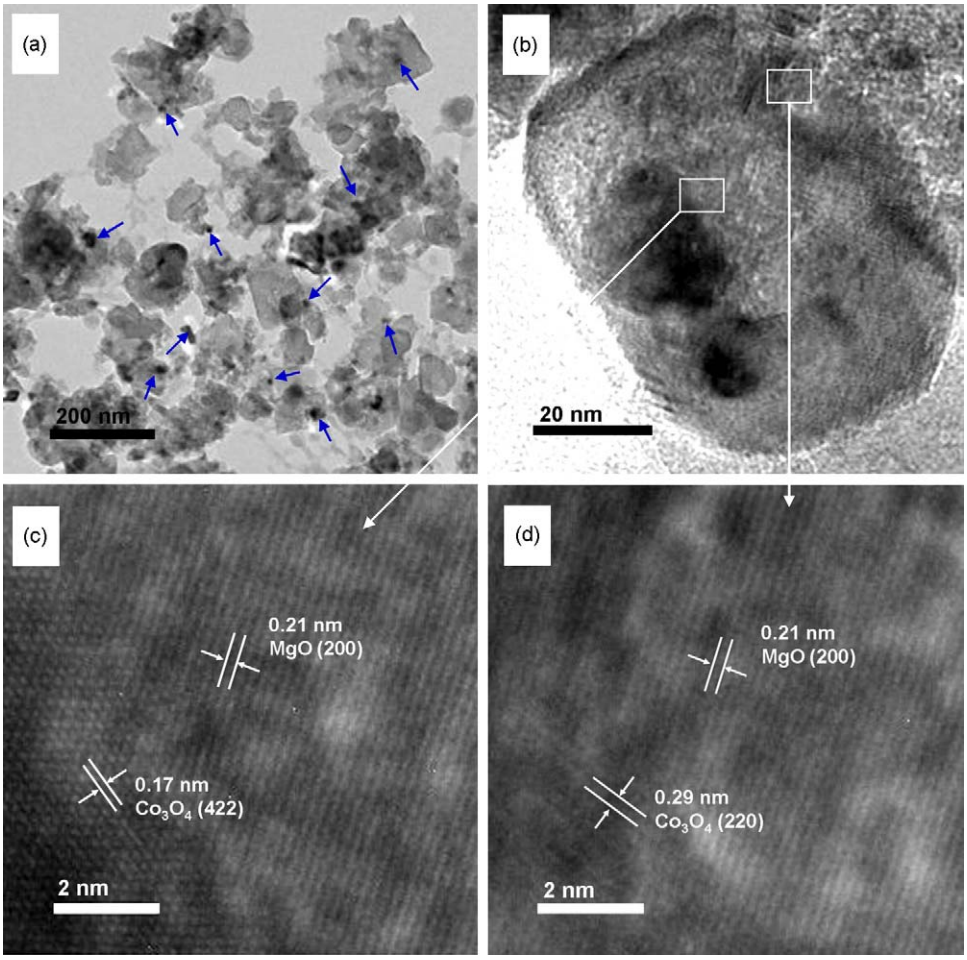

Fig. 2. TEM (a) and HRTEM (b and c) images of Co/MgO. The arrows in (a) point out the locations of cobalt oxide nanoparticles.

3.2. Catalytic activity

Fig. 5 shows the activities of cobalt catalysts loaded on different metal oxide supports for oxidative degradation of methylene blue (MB). The degradation speed of MB depends on the concentration of sulfate radicals generated, and hence it can be used to evaluate the performance of the supported cobalt catalysts as activators of PMS. The reactions were carried out in dilute solutions of MB (40 ppm) without any pH adjustment. The cobalt catalyst supported on MgO exhibits a much higher catalytic efficiency than that loaded on the rest of common oxide materials, ZnO, P25, ZrO_2, Al_2O_3 and SBA-15. It is remarkable that MB with a dilute starting concentration can be degraded completely in <7 min in a typical run when Co/MgO was used as the catalyst (Fig. 5a). Co/ZnO resulted in 91.5% of MB degradation after 30 min. Cobalt catalysts loaded on other supports (Al_2O_3, ZrO_2, P25, SBA-15) did not show satisfactory performance. The activity difference shown in Fig. 5 indeed correlates to the acid–base properties of the support materials. The most basic oxide, MgO, among the supports used in this work gives rise to the best catalyst. We presume that the surface basic sites from the MgO support can promote the formation of the surface Co–OH complex that can efficiently activate PMS during the reaction. Our studies further showed that the optimal loading of Co_3O_4 on MgO is 5 wt%, while the loading on other oxides seemed not having much effect on their performance (data not shown).

Fig. 6 displays the activities of Co/MgO catalysts prepared at different thermal treatment temperatures. It is found that the activities of Co/MgO catalysts treated at 600 °C (Fig. 6a) and 800 °C (Fig. 6b) are very close to each other. The former is slightly more active than the latter which could be probably due to their surface area difference as shown in Table 1. Co/MgO treated at a lower temperature of 400 °C has a relatively lower activity as it took 10 min to completely degrade MB under the same reaction conditions (Fig. 6c). Higher thermal treatment temperatures may give rise to a better interaction between cobalt oxide and the MgO support, and is thus helpful for the formation of surface Co–OH complex. Fig. 6 also shows the results from the control experiments using the homogeneous cobalt (dissolved $Co(NO_3)_2$), the physical mixture of Co_3O_4 and MgO, oxone alone (without the catalyst) and the Co/MgO catalyst alone (without oxone). The amounts of both homogeneous Co^{2+} ions in $Co(NO_3)_2$ and Co_3O_4 in the physical mixture were equivalent to that in the Co/MgO catalyst used for the reactions. Fig. 6d shows that the homogeneous Co^{2+} ions resulted in complete degradation of MB in 15 min under the same conditions. Thus the cobalt oxide on the supported Co/MgO catalysts prepared in this work is more active than the homogeneous Co^{2+} ions. They are also far more efficient than the unsupported Co_3O_4 catalyst. There is still 17.4% of MB remaining after 30 min when the physical mixture of Co_3O_4 and MgO was used as the catalyst (Fig. 6e). Meanwhile, the degradation occurred very slowly in the presence of PMS alone without a catalyst. Only around 18% of degradation was achieved after 30 min of reaction. In the presence of the Co/MgO catalyst but without PMS, the concentration of MB only decreased around 10% in the first few minutes and was then kept constant afterwards (Fig. 6g). Since a negligible extent of reaction occurred without PMS, the small drop in MB concentration could be due to the physical adsorption on the

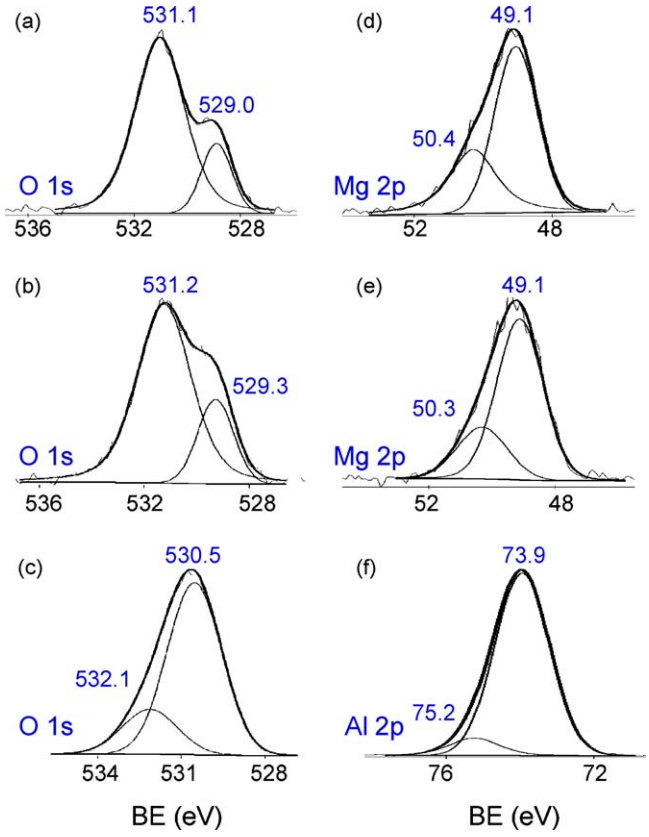

Fig. 3. XPS spectra of O 1s in (a) MgO, (b) Co/MgO, and (c) Co/Al_2O_3; Mg 2p in (d) MgO and (e) Co/MgO; and Al 2p in (f) Co/Al_2O_3.

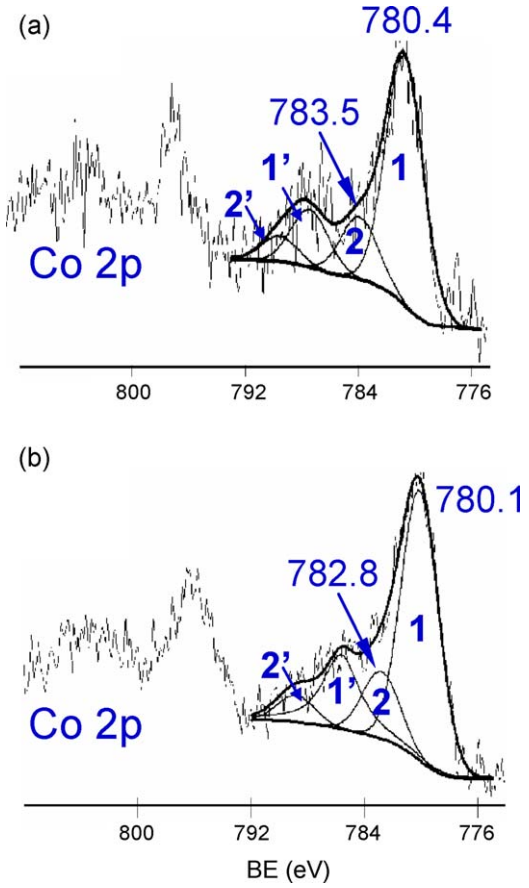

Fig. 4. XPS spectra of Co 2p in (a) Co/MgO and (b) Co/Al_2O_3.

catalyst surface. Therefore, it confirms that the quick decrease of MB concentration in the presence of both Co/MgO and PMS is due to the catalytic destruction of MB rather than the nondestructive adsorption of MB on the surface of the catalyst. In overall, the above results demonstrate the dominant role of the MgO support in promoting the activity of cobalt oxide catalyst for the generation of sulfate radicals from PMS. It is to note that a very low catalyst concentration of 0.05 g/L was used in our reactions. Based on the reaction data, the activity of the Co/MgO catalyst developed in this work is considered superior. The unsupported Co_3O_4 and Co_3O_4 supported on other materials usually required 30 min to 2 h for complete degradation of the organic pollutants even though higher catalyst concentrations were applied in those studies [10–12,16].

3.3. Heterogeneous activation of PMS by Co/MgO catalyst

Cobalt leaching has to be given great attention since homogeneous Co^{2+} ions are highly efficient for the activation of PMS. The previous reports show that the cobalt leaching from the heterogeneous Co_3O_4 and supported Co/TiO_2 and Co/Al_2O_3 catalysts were usually <1% even in acidic solutions [10,16]. In this study, it was noted that the leached cobalt concentration was very low since a low catalyst concentration (10 mg Co/MgO in 200 mL solution) was used in the reaction. In order to minimize the detection error from the instrument, larger amounts of catalysts were used in the reaction for the preparation of ICP samples. Typically, 100 mg of Co/MgO, 100 mg of Co/Al_2O_3 and 5 mg of Co_3O_4 were employed for reactions in 200 mL of the MB solution. The cobalt leaching levels during the reaction for the above three catalysts are shown in Fig. 7. These curves do not exhibit a clear trend in the leached cobalt ion concentrations in 30 min. It is found that the leached cobalt is only about 1–2% of the total cobalt present in Co/MgO catalyst. The concentration of the leached cobalt ion from Co/MgO is slightly higher than that from the unsupported Co_3O_4, but is lower than that from Co/Al_2O_3. Such difference between Co/MgO and Co/Al_2O_3 is consistent with the XRD results shown in Fig. 1 where the Co_3O_4 phase can be observed in Co/Al_2O_3 but not in Co/MgO due to a better dispersion and interaction of cobalt with the MgO support. The ICP results indicate

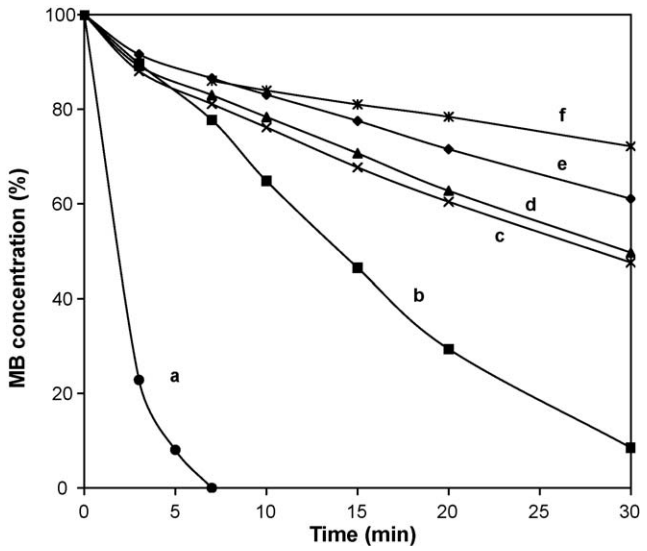

Fig. 5. Degradation of MB using different catalysts, (a) Co/MgO, (b) Co/ZnO, (c) Co/P25, (d) Co/ZrO_2, (e) Co/Al_2O_3, and (f) Co/SBA-15. Reaction conditions: 10 mg of catalysts (thermally treated at 600 °C) and 0.5 mM oxone in 200 mL of MB solution with a starting concentration of 40 ppm.

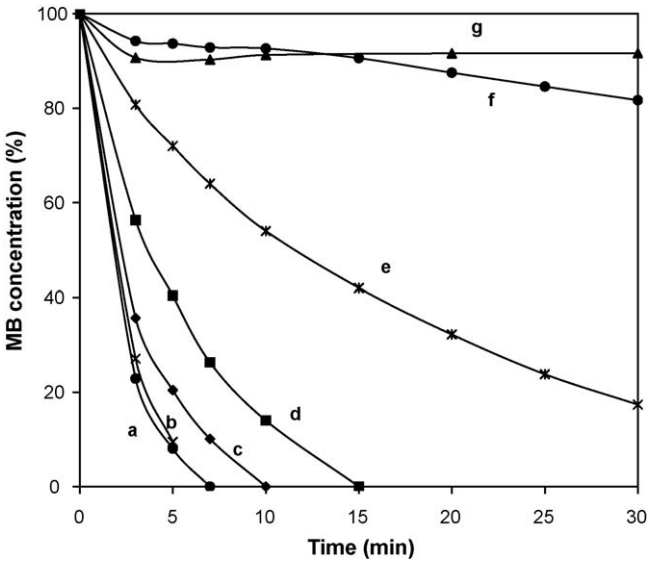

Fig. 6. Degradation of MB using different catalysts, (a) Co/MgO (thermally treated at 600 °C), (b) Co/MgO (thermally treated at 800 °C), (c) Co/MgO (thermally treated at 400 °C), (d) homogeneous Co^{2+} ions from dissolved $Co(NO_3)_2$ salt, and (e) physical mixture of MgO and Co_3O_4. Reactions conditions were the same as those indicated in Fig. 5. (f) 0.5 mM oxone, no catalyst, and (g) 10 mg of Co/MgO (thermally treated at 600 °C), no oxone; other reaction conditions were the same as those indicated in Fig. 5.

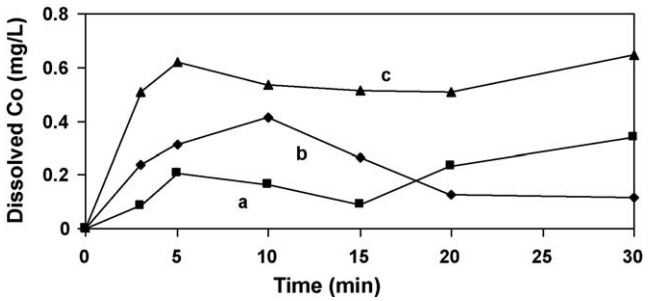

Fig. 7. The dissolved cobalt ion concentrations during the reaction with different catalysts, (a) Co_3O_4, (b) Co_3O_4/MgO, and (c) Co_3O_4/Al_2O_3. Reaction conditions: 100 mg of supported catalysts and 5 mg of unsupported Co_3O_4 were used; other reaction conditions were the same as those indicated in Fig. 5.

that there is no correlation between the activities of these catalysts and the dissolved cobalt ion concentrations. The leached cobalt ion concentrations reported by other groups involving heterogeneous activation of PMS were typically around 30–50 μg/L [10–12,16]. Taking into the account of low cobalt ion concentrations in the actual reaction (typically <50 μg/L) in this study, it is therefore suggested that the activation of PMS by Co/MgO catalyst is through the heterogeneous pathway. Apparently, the dispersed Co_3O_4 nanoparticles on MgO support function as a stable cobalt source to accelerate the generation of sulfate radicals from PMS, and the presence of the MgO support leads to a much higher acceleration efficiency.

In a homogeneous system, the cobalt ion catalyzed activation of PMS and degradation of organic compounds follow reactions (1)–(5) [2,7,13,38,39].

$$Co^{2+} + H_2O \rightarrow CoOH^+ + H^+ \quad (1)$$

$$CoOH^+ + HSO_5^- \rightarrow CoO^+ + SO_4^{\bullet -} + H_2O \quad (2)$$

$$CoO^+ + 2H^+ \rightarrow Co^{3+} + H_2O \quad (3)$$

$$Co^{3+} + HSO_5^- \rightarrow Co^{2+} + SO_5^{\bullet -} + H^+ \quad (4)$$

$$SO_4^{\bullet -} + \text{organicdyes} \rightarrow \text{intermediateproducts} \rightarrow CO_2 + H_2O \quad (5)$$

Two types of radicals can be generated based on reactions (2) and (4). With the oxidation of Co(II) to Co(III), PMS can be reduced to sulfate radical. The generation of PMS radicals involves the reduction of Co(III) to Co(II). The latter radical is a transient species and has weak oxidation ability. Sulfate radical is the major strong oxidant for degradation of organic dyes [3]. In heterogeneous cobalt catalyzed system, it is believed that the redox cycle of cobalt species occurring in Co_3O_4 (CoO and Co_2O_3) facilitates the radical generation. As shown in this work and also by other groups, the leaching of cobalt ions into solutions is minimal since the two different oxides of cobalt are bounded and can interact with each other [16]. Based on reaction (1), the formation of $CoOH^+$ ions is crucial for the radical generation in the subsequent step. MgO is considered as a solid base material and our XPS results also indicate that the surface of MgO is dominated by Mg–OH groups. As a result, the formation of $CoOH^+$ species is greatly facilitated on the MgO support, thus favoring the radical generation. Further, it has been demonstrated in this study that the supported Co/MgO catalyst has a much better efficiency for PMS activation than either the homogeneous Co^{2+} or the heterogeneous unsupported Co_3O_4 catalyst.

3.4. Stability of Co/MgO catalyst and degradation of other organic dyes

To evaluate the stability of the Co/MgO catalyst, three rounds of the MB degradation reaction was conducted with the recycling of the catalyst under the same reaction conditions. After the first run of reaction, catalyst was collected, washed thoroughly and dried before the second round. Several parallel reactions were conducted in the first and second runs to ensure that the catalyst amount was enough for the next run. As shown in Fig. 8, although the activity of the catalyst dropped slightly based on the data at 3 and 5 min, MB can still be completely degraded in 7 min in all the three runs. As the reaction solution was slightly acidic with a pH of about 4 due to the use of oxone, there may be some concern on the stability of the

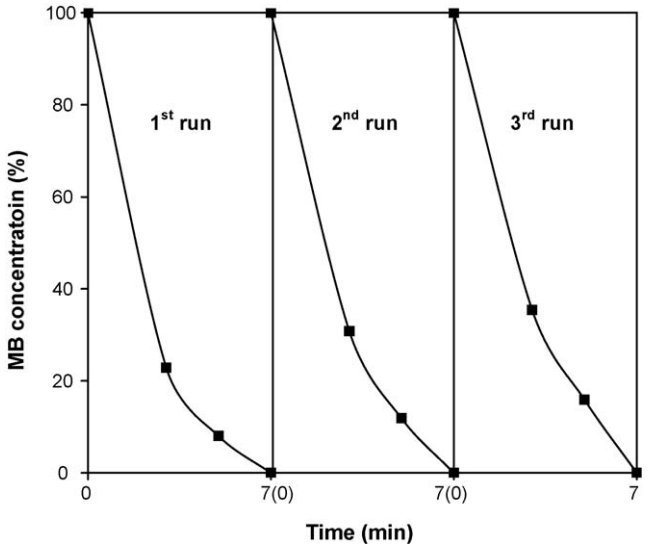

Fig. 8. Degradation of MB in consecutive runs using the recycled Co/MgO catalyst. After the first and second runs, the catalyst was collected, washed and dried; the reaction conditions were the same as those indicated in Fig. 5.

basic MgO support. The stability of the catalyst was further evaluated in more recycle runs. A larger catalyst amount (0.2 g) was used in the initial run and the reaction was repeated for 10 times. It was found that the complete degradation of MB always occurred within a few minutes. In the final run, the catalyst amount was reduced to 10 mg and the degradation of MB also occurred in <7 min. Therefore, it can be concluded that the Co/MgO catalyst is stable for more than 10 runs under the current reaction conditions.

The activity of the Co/MgO catalyst was also evaluated for degradation of the other two organic dyes, orange II (anionic, sodium salt) and malachite green (cationic, chloride salt) under the same reaction conditions. It has been found that the Co/MgO catalyst is also highly effective for degradation of both compounds in the dilute solutions without any pH adjustment. The time required for their complete degradation was both <6 min. The activity and stability evaluation of our catalysts for a wider range of organic pollutants are underway.

4. Conclusion

Cobalt oxide catalysts loaded on different support materials were prepared in this work. During the activation of PMS for degradation of MB, the Co/MgO catalyst exhibits a much better performance than those with other oxides including ZnO, P25, ZrO_2, Al_2O_3 and SBA-15 as the support materials. MgO with abundant surface hydroxyl groups may favor the formation of the surface $CoOH^+$ intermediate that can efficiently accelerate the generation of sulfate radicals from PMS. The Co/MgO catalyst has been found more active than both the unsupported Co_3O_4 catalyst and the homogeneous Co^{2+} ions. The complete degradation of methylene blue, orange II and malachite green with a dilute starting concentration all occurred with a very short duration of a few minutes. Based on the ICP analysis, the leached cobalt ions only reached a very dilute concentration, indicating a heterogeneous catalytic pathway. Therefore, the Co/MgO catalyst prepared in this work could be potentially used in advanced oxidation technologies towards the removal of organic pollutants.

Acknowledgements

The authors gratefully acknowledge the research funding support from Ministry of Education, Singapore (ARC25/08). Zhang W. acknowledges the research scholarship from Nanyang Technological University. We also thank Dr. Y.H. Yang's group for providing us the SBA-15 support material.

References

[1] G.P. Anipsitakis, D.D. Dionysiou, Appl. Catal. B: Environ. 54 (2004) 155.
[2] G.P. Anipsitakis, D.D. Dionysiou, Environ. Sci. Technol. 37 (2003) 4790.
[3] G.P. Anipsitakis, D.D. Dionysiou, Environ. Sci. Technol. 38 (2004) 3705.
[4] G.P. Anipsitakis, D.D. Dionysiou, M.A. Gonzalez, Environ. Sci. Technol. 40 (2006) 1000.
[5] Z.Y. Yu, L. Kiwi-Minsker, A. Renken, J. Kiwi, J. Mol. Catal. A: Chem. 252 (2006) 113.
[6] J. Fernandez, P. Maruthamuthu, A. Renken, J. Kiwi, Appl. Catal. B: Environ. 49 (2004) 207.
[7] J. Kim, J.O. Edwards, Inorg. Chim. Acta 235 (1995) 9.
[8] J. Fernandez, V. Nadtochenko, J. Kiwi, Chem. Commun. (2003) 2382.
[9] P. Raja, M. Bensimon, U. Klehm, P. Albers, D. Laub, L. Kiwi-Minsker, A. Renken, J. Kiwi, J. Photochem. Photobiol. A: Chem. 187 (2007) 332.
[10] Q.J.H. Choi, Y.J. Chen, D.D. Dionysiou, Appl. Catal. B: Environ. 77 (2008) 300.
[11] Q.J. Yang, H. Choi, D.D. Dionysiou, Appl. Catal. B: Environ. 74 (2007) 170.
[12] X.Y. Chen, J.W. Chen, X.L. Qiao, D.G. Wang, X.Y. Cai, Appl. Catal. B: Environ. 80 (2008) 116.
[13] J.G. Muller, P. Zheng, S.E. Rokita, C.J. Burrows, J. Am. Chem. Soc. 118 (1996) 2320.
[14] P.K. Sahoo, H.S. Samantaray, R.K. Samal, J. Appl. Polym. Sci. 32 (1986) 5693.
[15] R.K. Samal, H.S. Samantaray, R.N. Samal, J. Appl. Polym. Sci. 37 (1989) 3085.
[16] G.P. Anipsitakis, E. Stathatos, D.D. Dionysiou, J. Phys. Chem. B 109 (2005) 13052.
[17] V.R. Choudhary, M.Y. Pandit, Appl. Catal. 71 (1991) 265.
[18] T. Lopez, I. Garciacruz, R. Gomez, J. Catal. 127 (1991) 75.
[19] M.A. Aramendia, V. Borau, C. Jimenez, J.M. Marinas, A. Porras, F.J. Urbano, J. Mater. Chem. 6 (1996) 1943.
[20] A. Houas, H. Lachheb, M. Ksibi, E. Elaloui, C. Guillard, J.M. Herrmann, Appl. Catal. B: Environ. 31 (2001) 145.
[21] T. Umebayashi, T. Yamaki, S. Tanaka, K. Asai, Chem. Lett. 32 (2003) 330.
[22] S. Lakshmi, R. Renganathan, S. Fujita, J. Photochem. Photobiol. A: Chem. 88 (1995) 163.
[23] T. Ohno, M. Akiyoshi, T. Umebayashi, K. Asai, T. Mitsui, M. Matsumura, Appl. Catal. A: Gen. 265 (2004) 115.
[24] Y.Z. Chen, C.T. Yang, C.B. Ching, R. Xu, Langmuir 24 (2008) 8877.
[25] Y.C. Lou, Q.H. Tang, H.R. Wang, B.T. Chia, Y. Wang, Y.H. Yang, Appl. Catal. A: Gen. 350 (2008) 118.
[26] D.L. Trimm, Design of Industrial Catalysts, Elsevier, Amsterdam, 1980.
[27] J.F. Le Page, Applied Heterogeneous Catalysis – Design, Manufacture, Use of Solid Catalysts, Technip, Paris, 1987.
[28] F.A. Cotton, G. Wilkinson, Advanced Inorganic Chemistry, 4th ed., John Wiley & Sons, New York, 1980.
[29] J.F. Moulder, W.F. Stickle, P.E. Sobol, K.D. Bomben, Handbook of X-ray Photoelectron Spectroscopy, Perkin Elmer, Eden Prairie, 1992.
[30] C.H. Sun, J.C. Berg, Adv. Colloid Interface Sci. 105 (2003) 151.
[31] M.A. Blesa, A.D. Weisz, P.J. Morando, J.A. Salfity, G.E. Magaz, A.E. Regazzoni, Coord. Chem. Rev. 196 (2000) 31.
[32] M.E. Labib, Colloids Surf. 29 (1988) 293.
[33] B.M. Reddy, B. Chowdhury, E.P. Reddy, A. Fernandez, Appl. Catal. A: Gen. 213 (2001) 279.
[34] T.L. Barr, S. Seal, L.M. Chen, C.C. Kao, Thin Solid Films 253 (1994) 277.
[35] I. Shimizu, Y. Setsuhara, S. Miyake, M. Kumagai, K. Ogata, M. Kohata, K. Yamaguchi, Surf. Coat. Technol. 131 (2000) 187.
[36] R. Xu, H.C. Zeng, Chem. Mater. 15 (2003) 2040.
[37] I. Zacharaki, C.G. Kontoyannis, S. Boghosian, A. Lycourghiotis, C. Kordulis, Catal. Today 143 (2009) 38.
[38] Z.M. Zhang, J.O. Edwards, Inorg. Chem. 31 (1992) 3514.
[39] R.C. Thompson, Inorg. Chem. 20 (1981) 1005.